Outcoupling-Enhanced Flexible Organic Light-Emitting Diodes on Ameliorated Plastic Substrate with Built-in Indium–Tin-Oxide-Free Transparent Electrode

Heng-Yang Xiang,[†,‡] Yan-Qing Li,[*,†,‡] Lei Zhou,[†,‡] Hao-Jun Xie,[†,‡] Chi Li,[†,‡] Qing-Dong Ou,[†,‡] Lin-Sen Chen,[‡,§] Chun-Sing Lee,[∥] Shuit-Tong Lee,[†,‡] and Jian-Xin Tang[*,†,‡]

[†]Institute of Functional Nano & Soft Materials (FUNSOM), Jiangsu Key Laboratory for Carbon-Based Functional Materials & Devices, and [‡]Collaborative Innovation Center of Suzhou Nano Science and Technology, Soochow University, Suzhou 215123, China, [§]College of Physics Optoelectronics and Energy, Soochow University, Suzhou 215006, China, and [∥]Center of Super-Diamond and Advanced Films, Department of Physics and Materials Science, City University of Hong Kong, Hong Kong SAR, China

ABSTRACT Enhancing light outcoupling in flexible organic light-emitting diodes (FOLEDs) is an important task for increasing their efficiencies for display and lighting applications. Here, a strategy for an angularly and spectrally independent boost in light outcoupling of FOLEDs is demonstrated by using plastic substrates with a low refractive index, consisting of a bioinspired optical coupling layer and a transparent conductive electrode composed of a silver network. The good transmittance to full-color emission (>94% over the whole visible wavelength range), ultralow sheet resistance to carrier injection (<5 Ω sq^{-1}), and high tolerance to mechanical bending of the ameliorated plastic substrates synergistically optimize the device performance of FOLEDs. The maximum power efficiencies reach 47, 93, 56, and 52 lm W^{-1} for red, green, blue, and white emissions, which are competitive with similarly structured OLEDs fabricated on traditional indium–tin-oxide (ITO) glass. This paradigm for light outcoupling enhancement in ITO-free FOLEDs offers additional features and design freedoms for highly efficient flexible optoelectronics in large-scale and low-cost manufacturing without the need for a high-refractive-index plastic substrate.

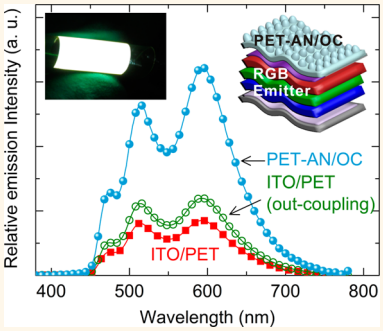

KEYWORDS: flexible OLEDs · flexible transparent conductors · light outcoupling · plastic substrates

Flexible organic light-emitting diodes (FOLEDs) are an emerging display technology that enables amazing and efficient displays and lighting panels in mobile devices, televisions, smart windows, and other bendable wearable electronics.[1−4] To realize highly efficient FOLEDs, two major challenges have to be addressed. First, transparent conductive electrodes (TCEs) with excellent electrical, optical, and mechanical properties have to be achieved. Second, the light outcoupling efficiency in FOLEDs should be as efficient as possible for the extraction of the internally created photons to the forward hemisphere.

The most commonly used indium–tin-oxide (ITO) TCE is unsuitable for use in FOLEDs and other flexible devices due to its brittleness, scarcity of indium element, and high-cost and high-temperature processing.[5,6] Accordingly, potential alternative TCEs have been extensively pursued for the development of high-performance ITO-free flexible optoelectronic devices,[7−20] including conductive polymers,[5,7] graphene,[8,9] carbon nanotubes (CNTs),[10,11] metallic nanowires (NWs),[12−15] dielectric/metal/dielectric (DMD) composite electrodes,[16−18] and metal grids.[19−25] Among these emerging TCEs, printed Ag grids produced by inkjet printing,[23] direct ink writing,[24] or screen-printing[25] have attracted much attention due to their good mechanical flexibility, superior optical transmittance and electrical conductivity, and low-cost solution processing compatibility. However, the balance

* Address correspondence to jxtang@suda.edu.cn (J.-X. Tang), yqli@suda.edu.cn (Y.-Q. Li).

Received for review May 10, 2015 and accepted July 4, 2015.

Published online July 04, 2015
10.1021/acsnano.5b02826

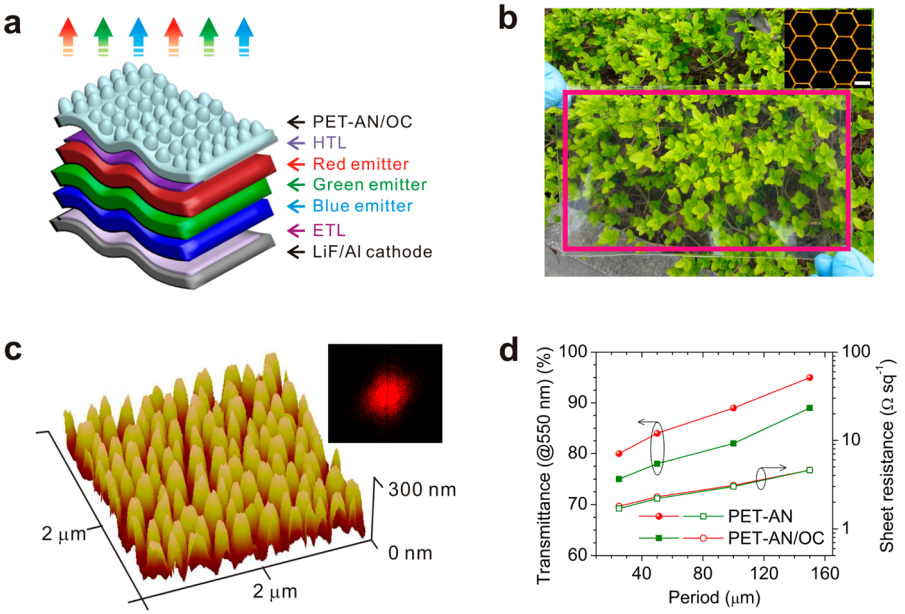

Figure 1. Device structure and characteristics of an ameliorated PET substrate with a built-in Ag network electrode (hereafter termed PET-AN/OC). (a) Schematic illustration of FOLEDs using PET-AN/OC as a transparent conductive electrode. (b) Photograph of a large-area PET-AN/OC (size: 20 cm × 10 cm). Inset: Magnified optical image of the hexagonal Ag network (period = 150 μm, groove depth = 3 μm, and line width = 3 μm), showing the optical transmittance of ~94% at the visible wavelength region. Scale bar = 150 μm. (c) 3D atomic force microscopy (AFM) images of moth-eye nanostructures constructed on PET substrates with period = 200 nm, groove depth = 300 nm, fill factor = 0.6. Inset shows the fast Fourier transform (FFT) pattern. (d) Measured optical transmittance (at 550 nm) and sheet resistance for PET-ANs and PET-AN/OCs with various Ag network periods.

between optical transparency and electrical conductivity, the chemical/mechanical stabilities, and the fabrication process of these emerging TCEs need further improvement before they can be practically used in flexible optoelectronic devices.

Regardless of the rapid development of new flexible TCEs, the majority of the internally generated light of FOLEDs in a standard substrate emitting architecture with an ITO electrode on the substrate is trapped in waveguide and substrate modes due to the optical confinement and total internal reflection, which are induced by the large difference in the refractive indices n between the organic layers ($n_{org} \approx 1.6-1.8$), ITO ($n_{ITO} \approx 1.8$), the plastic and/or glass substrate ($n_{sub} \approx 1.5$), and air ($n_{air} \approx 1$).[26] The light outcoupling efficiency of FOLEDs without outcoupling enhancement is typically limited to ~20%, suggesting considerable opportunity for a substantial increase in external quantum efficiency (EQE) and power efficiency (PE). Therefore, numerous studies have been dedicated to the realization of novel device architectures for improving the light outcoupling capabilities, including the use of high-refractive-index substrates, low-index dielectric grids, a random scattering layer, or deterministic aperiodic nanostructures.[2,27−34] Among them, many techniques rely on the use of high-refractive-index substrates to match the refractive index of the ITO layer for the outcoupling enhancement of the trapped light.[28,34,35] However, flexible plastic substrates [*e.g.*, polyethylene terephthalate (PET)] widely used for FOLEDs have a low refractive index ($n_{sub} < 1.6$), which is unfortunately mismatched with that of ITO. A new light outcoupling strategy is thus highly desirable to realize high-performance FOLEDs on low-refractive-index flexible plastic substrates to boost their overall efficiency for their full potential in flexible displays and solid-state lighting.

Here, we present an alternative route for angularly and spectrally independent enhancement of light outcoupling in FOLEDs that does not rely on high-refractive-index flexible plastic substrates (Figure 1). In these flexible devices, the key feature is an ameliorated low-refractive-index PET substrate that consists of a built-in TCE of a Ag network (AN) and a bioinspired optical coupling (OC) layer of moth-eye nanostructures (hereafter termed PET-AN/OC), enabling the broadband transmittance to full-color emission (>94% over the whole visible wavelength range), ultralow sheet resistance to carrier injection (<5 Ω sq^{-1}), and high tolerance to mechanical bending. The highly enhanced light extraction can be realized without alternating the electrical properties of FOLEDs. As a result, FOLEDs with PE values of 47, 9, 56, and 52 lm W^{-1} for red, green, blue, and white emissions, respectively, are demonstrated, which are competitive with their counterparts fabricated on standard ITO-coated glass substrates.

RESULTS AND DISCUSSION

Ameliorated Plastic Substrate for Carrier Conduction and Light Outcoupling. Preparation of the PET-AN/OC substrate is

schematically summarized in Supporting Figure S1. One side of a PET substrate was first coated with a UV-curable resin, which was then nanoimprinted to form a hexagonal network of shallow grooves of about 3 μm in width and 3 μm in depth. The grooves were filled with a silver ink by the doctor blade method. The Ag network was then formed by annealing at 100 °C for 6 min. The other side of the PET substrate was subsequently coated with the same UV-curable resin and imprinted with a moth-eye nanostructured polydimethylsiloxane mold. The PET-AN/OC substrate is finally finished by UV-curing of the resin.

Figure 1b shows an optical image of a 20 cm × 10 cm PET-AN/OC substrate put in front of a photograph. The difficulty in discerning the PET-AN/OC substrate shows its high optical transparency. The inset shows a magnified image of the silver network with a period of 150 μm, whose discrepancy from the visible wavelength also contributes to the high transparency of the PET-AN/OC substrate. Figure 1c shows an atomic force microscopy (AFM) image of the bioinspired moth-eye nanostructure (period = 200 nm, duty cycle = 0.6, and groove depth = 300 nm) prepared as reported previously.[36] Moreover, the character of the extended periodicity distribution as observed in the fast Fourier transform (FFT) pattern (Figure 1c, inset) reveals the formation of quasi-periodic structures, which would be favorable for the light outcoupling enhancement with broadband response.[29,31,36,37] As depicted in Figure 1d, the combination of periodic AN electrode and the moth-eye OC layer can result in the optimization of optical transmittance and electrical conductivity simultaneously. Compared to the PET substrate only with a built-in TCE of a Ag network (hereafter termed PET-AN), the optical transmittance of a flexible PET-AN/OC substrate can be enhanced by over 5% without sacrificing the electric conductivity (Figure 1d and Supporting Figure S2). For instance, the incorporation of the moth-eye nanostructured OC layer increases the transmittance of PET-AN/OCs from ~87% to ~94% in the visible wavelength range of 400−800 nm, while the sheet resistance remains as low as 5 Ω sq^{-1} (Figure 1c). Optical and electrical properties of PET-AN/OCs are comparable and even superior to other TCEs reported in the literature (ITO-PET, graphene, metal NWs, CNTs, *etc.*).[38−42] In addition to the transmittance enhancement, the amount of light scattering present in PET-AN/OCs with various periods was characterized as compared to those of bare PET and ITO-coated PET (ITO/PET) with the same moth-eye OC layer (Supporting Figure S2). It is clear that the haze values of PET-AN/OCs depend strongly on the periods of the Ag network. However, the PET-AN/OC with a period of 150 μm exhibits an averaged transmittance haze of ~5.4% over the range of 400−800 nm, which is comparable to that of ITO/PET and bare PET substrates (Supporting Figure S2). This result indicates that the PET-AN/OC is capable of keeping the substrate transparency with a small fraction of diffusely scattered light, which is one crucial feature in high-resolution display applications. Furthermore, the PET-AN/OC substrates show good stability against atmospheric environment and a high tolerance to repeated bending (Supporting Figure S3). It is evident that the PET-AN/OC substrates keep nearly the same sheet resistance upon exposure to ambient conditions without any extra protection means (Figure S3a). Compared to the ITO/PET substrate, the PET-AN/OC exhibits a better mechanical stability upon repeated bending. The FOLEDs using PET-AN/OCs show a small decrease in efficiency under repeated bending, whereas the corresponding devices on ITO/PET are quickly damaged to failure due to the cracking in the brittle ITO (Figure S3b).

Performance of Monochrome FOLEDs. The flexible plastic substrates of PET-AN/OC and ITO/PET (with and without the same moth-eye outcoupling layer) were used as substrates for making FOLEDs (12 mm × 12 mm) of different colors. Taking into account the balance between optical transmittance and electrical conductivity, the PET-AN/OC with a period of 150 μm was used for the device fabrication in this study. Figure 1a gives a schematic illustration of the device structure. A 80 nm thick poly(3,4-ethylenedioxythiophene):poly(styrenesulfonate) (PEDOT:PSS) layer was first spin-coated on the flexible plastic substrate as a hole injection layer (HIL), which enables efficient hole injection into organic emitters. NPB, TCTA, and TmPyPB (see Methods section for material compositions) were used as the hole transport layer (HTL), electron/exciton blocking layer (EBL), and electron transport/hole blocking layer (ETL), respectively. The ultrathin (0.1 nm) and nondoped organic red, green, or blue emitter of Ir(MDQ)$_2$(acac), Ir(ppy)$_2$(acac), or FIrpic was sandwiched between the EBL and ETL. The use of ultrathin nondoped emitters in various devices simplifies the device fabrication process with comparable efficiency by avoiding the concentration quenching effect in the doping-based devices and the requirement of precise control of the deposition rate of host and dopant materials.[43,44] The details of the device structures and materials can be found in the Methods section.

Current density−luminance−voltage (*J*−*L*−*V*) characteristics of FOLEDs with red, green, and blue emissions are shown in Figures 2a, e, and i, respectively. It is evident that the use of PET-AN/OCs causes a reduced driving voltage as compared to those using the traditional ITO/PET substrates, which is ascribed to the smaller sheet resistance of PET-AN/OC (<5 Ω sq^{-1}) than that of ITO/PET (~20 Ω sq^{-1}). It is also observed that the *J*−*V* curves of FOLEDs on ITO/PET substrates with and without an outcoupling layer are nearly coincident, indicating that the use of a moth-eye OC layer on the outer surface of flexible plastic substrates has no influence on the electrical properties of the devices.

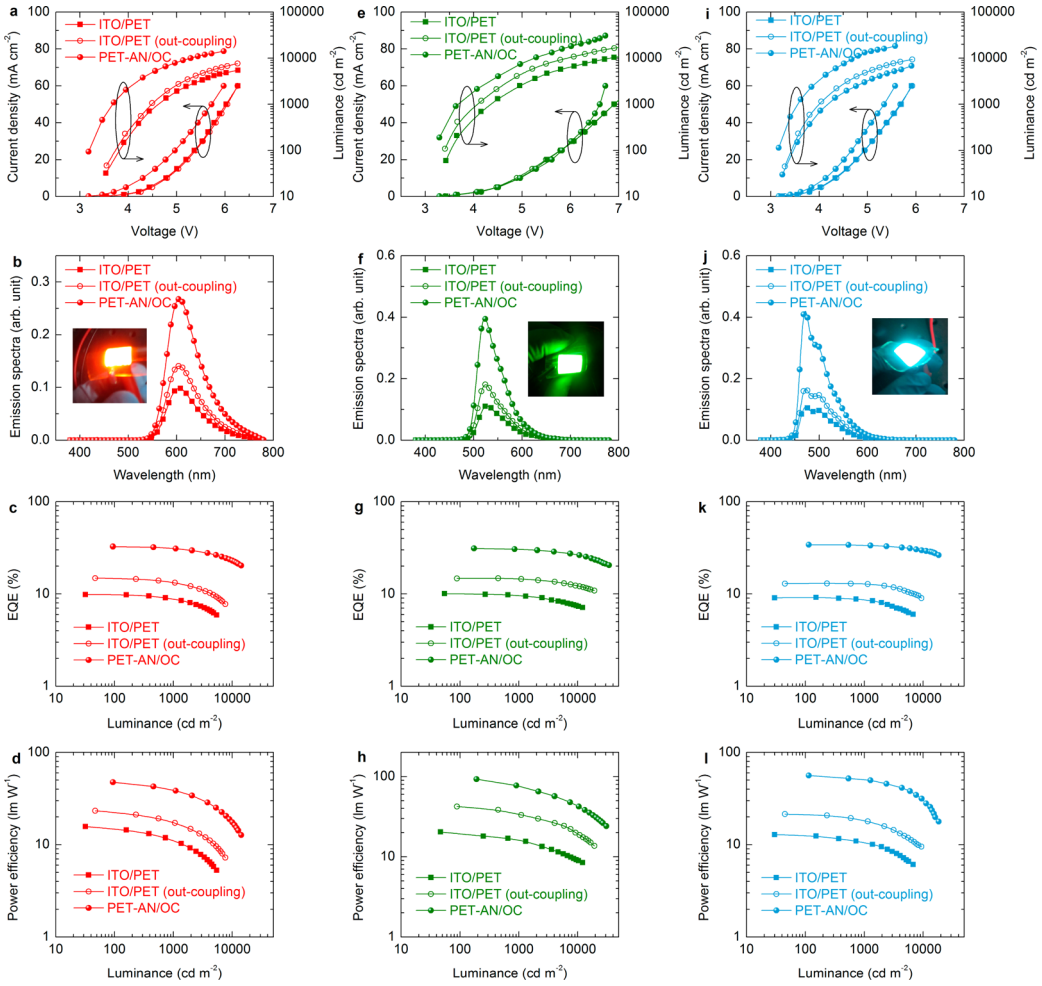

Figure 2. Device performance of red, green, and blue FOLEDs using PET-AN/OCs as compared to those on ITO/PET with and without the moth-eye outcoupling layer. (a–d) Current density–luminance–voltage characteristics (a), electroluminescence (EL) spectra at the normal direction at 20 mA cm^{-2} (b), and external quantum efficiency (EQE) (c) and power efficiency (d) as a function of luminance for red FOLEDs. Inset in (b) is a photograph of a red FOLED (12 mm × 12 mm) using PET-AN/OC. (e–h) Performance characteristics of green FOLEDs. (i–l) Performance characteristics of blue FOLEDs.

The photographs (insets in Figure 2b, f, and j) of FOLEDs using PET-AN/OCs (12 mm × 12 mm) show the extremely uniform light distribution for red, green, and blue emissions, indicating the good electrical conduction and carrier injection of PET-AN/OCs as an anode in FOLEDs. More importantly, the luminance of FOLEDs using PET-AN/OCs is significantly enhanced as compared to those on ITO/PET substrates with and without a moth-eye outcoupling layer (Figure 2a, e, and i).

As extensively studied using ultrathin metal films as alternative TCEs to replace ITO electrode, a strong optical microcavity is inevitably formed between the semitransparent metal film and the highly reflective metal rear electrode, which would cause spectral distortion and outcoupling enhancement at limited viewing angles.[2,16–18] Accordingly, optical effects of the PET-AN/OC substrate on emission spectra of FOLEDs were characterized. Figure 2b, f, and j clearly show that the incorporation of the PET-AN/OC substrate causes a negligible microcavity effect and, hence, does not distort or shift the electroluminescence (EL) spectra in the visible wavelength region. Instead, the emission intensities of various FOLEDs fabricated on PET-AN/OC substrates are much higher than those on ITO/PET substrates.

Figure 2 and Supporting Figure S4 present the measured EQE, PE, and current efficiency (CE) characteristics of various FOLEDs, and the key efficiency values are summarized in Table 1. For comparison, the performance of OLEDs on an ITO-coated glass substrate is also provided. It is shown that the use of PET-AN/OCs in FOLEDs causes a dramatic boost in device efficiency as compared with those on ITO/PET and ITO/glass substrates. For example, FOLEDs using PET-AN/OCs yield the maximum EQE values of 32.6%, 31.2%, and 34.2% for red, green, and blue emissions, respectively. The corresponding PE values are 38.5, 77.2, and 49.9 lm W^{-1} at a luminance of 1000 cd m^{-2}, which are significantly enhanced by a factor of ~2.2, ~2.3, and ~2.7 times that of the devices on an ITO/PET substrate with the same outcoupling layer, respectively. These results strongly demonstrate the potential of

TABLE 1. Performance Comparison of FOLEDs Using Various Substrates[a]

	device structure	CE_{max} [cd A^{-1}]	CE_{1000} [cd A^{-1}]	PE_{max} [lm W^{-1}]	PE_{1000} [lm W^{-1}]	EQE_{max} [%]	EQE_{1000} [%]
red	ITO/PET	16.0 ± 0.6	14.3 ± 0.7	15.7 ± 0.4	11.2 ± 0.6	9.8 ± 0.6	8.5 ± 0.7
	ITO/PET (outcoupling)	23.5 ± 0.7	21.2 ± 0.8	23.3 ± 0.6	17.3 ± 0.7	14.8 ± 0.9	12.8 ± 0.5
	PET-AN/OC	47.0 ± 1.5	43.8 ± 1.3	47.5 ± 0.9	38.5 ± 1.4	32.6 ± 1.1	29.3 ± 1.2
	ITO/glass	28.1 ± 0.6	27.4 ± 0.4	30.1 ± 0.7	24.1 ± 0.5	19.8 ± 0.4	18.2 ± 0.5
green	ITO/PET	27.2 ± 1.4	26.1 ± 1.3	22.5 ± 1.5	15.8 ± 1.4	10.1 ± 0.7	9.4 ± 0.6
	ITO/PET (outcoupling)	45.3 ± 1.7	43.9 ± 1.8	42.3 ± 1.8	33.2 ± 1.6	14.7 ± 1.2	13.5 ± 1.0
	PET-AN/OC	95.5 ± 3.1	90.3 ± 2.2	92.9 ± 2.5	77.2 ± 2.9	31.2 ± 1.5	29.1 ± 1.7
	ITO/glass	62.5 ± 3.9	60.2 ± 2.7	61.4 ± 3.8	59.0 ± 2.5	18.1 ± 1.7	17.4 ± 1.6
blue	ITO/PET	15.2 ± 0.4	14.1 ± 0.6	12.9 ± 0.5	10.2 ± 0.4	9.1 ± 0.6	7.8 ± 0.4
	ITO/PET (outcoupling)	23.6 ± 0.8	23.1 ± 0.7	21.5 ± 0.7	18.8 ± 0.9	12.9 ± 1.0	11.8 ± 0.9
	PET-AN/OC	57.0 ± 1.3	53.1 ± 1.6	56.2 ± 1.4	49.9 ± 1.7	34.2 ± 1.1	29.6 ± 0.9
	ITO/glass	37.4 ± 1.4	34.0 ± 1.6	38.0 ± 1.6	35.5 ± 1.7	16.3 ± 1.3	15.1 ± 1.5
white	ITO/PET	13.2 ± 0.8	12.9 ± 0.7	11.1 ± 0.7	9.2 ± 0.5	10.4 ± 0.6	8.8 ± 0.5
	ITO/PET (outcoupling)	19.2 ± 0.5	18.6 ± 0.5	16.8 ± 0.7	14.0 ± 0.7	14.4 ± 0.6	13.1 ± 0.5
	PET-AN/OC	57.9 ± 1.7	55.8 ± 1.8	52.2 ± 1.6	47.8 ± 1.6	31.5 ± 1.6	29.6 ± 1.5
	ITO/glass	33.2 ± 1.1	31.9 ± 0.9	34.1 ± 0.8	33.2 ± 0.7	18.4 ± 0.9	17.1 ± 0.6

[a] The average current efficiency (CE), EQE, and PE values at the maximum and at a luminance of 1000 cd m^{-2} are obtained from at least 12 devices.

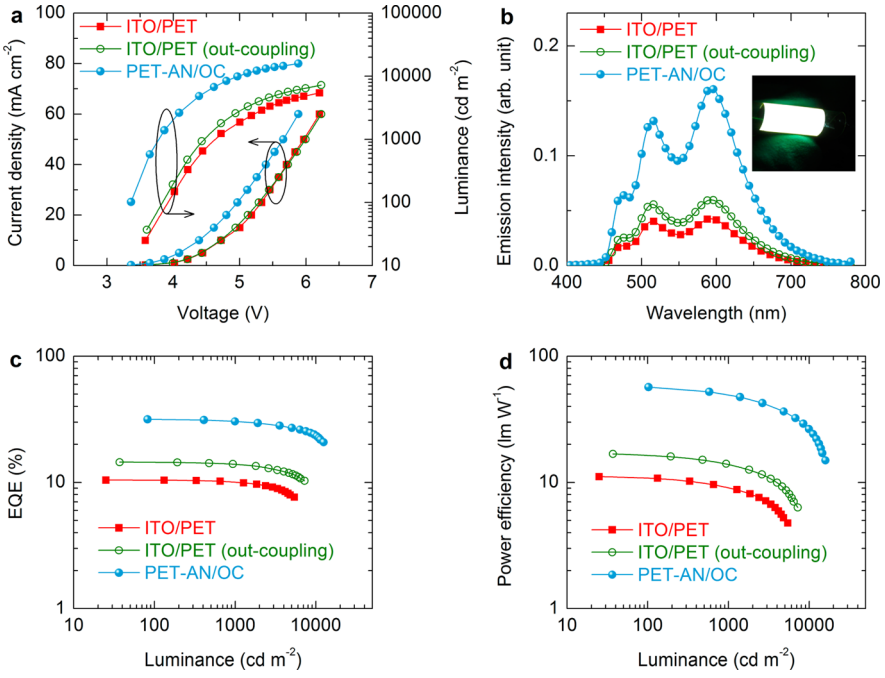

Figure 3. Performance characteristics of white FOLEDs on various flexible substrates. (a) *J*−*L*−*V* characteristics. (b) EL spectra of various white FOLEDs at a current density of 20 mA cm^{-2} in the normal direction. Inset: Photograph of a white FOLED (12 mm × 12 mm) using PET-AN/OC. (c) EQE as a function of luminance. (d) Power efficiency as a function of luminance.

PET-AN/OCs as an alternative TCE to replace ITO in FOLEDs.

Performance of White FOLEDs. To further elucidate the characteristics of PET-AN/OCs, white FOLEDs were fabricated, where ultrathin nondoped red, green, and blue emissive layers were adopted with a structure of anode/PEDOT:PSS (80 nm)/NPB (40 nm)/TCTA (13 nm)/$Ir(MDQ)_2(acac)$ (0.1 nm)/TCTA (1 nm)/$Ir(ppy)_2(acac)$ (0.05 nm)/TCTA (1 nm)/FIrpic (0.1 nm)/TmPyPB (40 nm)/LiF (1 nm)/Al (100 nm). Figure 3a shows *J*−*L*−*V* curves of the white FOLEDs on PET-AN/OC and ITO/PET substrates with and without an outcoupling layer. Similar to the cases of monochrome FOLEDs in Figure 3a, the use of PET-AN/OCs results in the enhanced electrical property and higher luminance than that on ITO/PET substrates. The picture of white FOLEDs using PET-AN/OC in Figure 3b shows uniform white light emission. Figure 3a presents the EL spectra of white FOLEDs constructed on PET-AN/OC and ITO/PET substrates at 20 mA cm^{-2} in the normal direction. It is apparent that the emission spectra on various flexible substrates are almost identical, showing a wavelength-independent output response of PET-AN/OCs for white light emission.

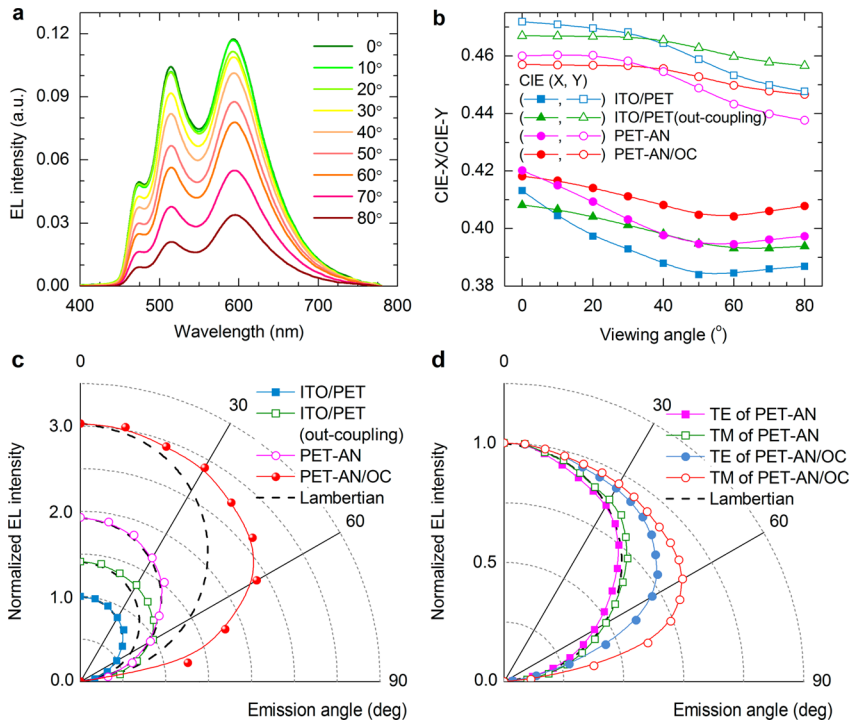

Figure 4. Angular dependence of emission characteristics of white FOLEDs. (a) EL spectra *versus* viewing angle for white FOLEDs using PET-AN/OC. (b) CIE color coordinates as a function of viewing angles for white FOLEDs on various flexible substrates. (c) Angular dependence of light intensity for white FOLEDs on various flexible substrates. (d) Simulation of angle-dependent emission intensities of TE and TM polarized light for white FOLEDs on PET-AN and PET-AN/OC substrates, which were calculated with the finite-difference time-domain (FDTD) method. The ideal Lambertian emission patterns are shown in (c) and (d) with dashed lines as a guide to the eye.

Figure 3c and d plot EQE and PE characteristics of the white FOLEDs on PET-AN/OC and ITO/PET substrates. As summarized in Table 1, white FOLEDs on PET-AN/OC yield a CE of 55.8 cd A^{-1}, an EQE of 29.6%, and a PE of 47.8 lm W^{-1} at a luminance of 1000 cd m^{-2}, which are almost 3-fold higher than those on ITO/PET with an outcoupling layer. These results indicate that the PET-AN/OC not only serves as an efficient conductive channel for charge transport but also facilitates the light outcoupling.

Figure 4 displays the angular dependence of emission characteristics. It is interesting to note in Figure 4a that white FOLEDs using PET-AN/OC exhibit the almost identical emission spectra with respect to the increase in the viewing angle, yielding a consistent white color. Correspondingly, the angular dependences of Commission Internationale d'Eclairage (CIE) coordinates (X, Y) of white FOLEDs on various flexible substrates are compared in Figure 4b, showing the superior stability of PET-AN/OC-based devices with increasing viewing angle. Additionally, the use of PET-AN/OC leads to a stronger emission at a large viewing angle rather than that on an ITO/PET substrate with a Lambertian intensity distribution (Figure 4c), which is consistent with the simulated results of transverse electric (TE) and transverse magnetic (TM) modes with the finite-difference time-domain (FDTD) method (Figure 4d). Through the experimental characterization and theoretical simulations, the enhanced light emission at wider viewing angles for white FOLED using PET-AN/OC is ascribed to the capability of the quasi-omnidirectional light outcoupling of a biomimetic moth-eye coupling layer at the air/PET interface, which induces the redirected emission for the broadband wavelengths over all azimuthal directions.[31,33,45] These results indicate that white FOLEDs using PET-AN/OC will be applicable to high-quality full-color flexible displays and solid-state lighting due to the omnidirectional color uniformity.

Enhancement Mechanism of Light Outcoupling Using PET-AN/OC. To elucidate the outcoupling enhancement mechanisms of FOLEDs using PET-AN/OC, emission behaviors of various FOLEDs were analyzed based on the optical modeling calculations (see Methods section for details of the optical modeling). Figure 5 presents the simulated distributions of the field intensities of TM and TE polarized light in various layers of FOLEDs on PET-AN/OC and ITO/PET substrates by using the FDTD method.[29,46] As qualitatively shown in Figure 5a and b, the removal of the ITO electrode in FOLEDs results in the relocation of the major field distribution of the TE-mode polarized light from the ITO layer into the plastic substrate, implying a substantial suppression of waveguide mode and a significant gain of substrate mode. The change in the field distributions is due to the improved refractive-index matching between the PET-AN/OC substrate ($n_{sub} \approx 1.5$) and the PEDOT:PSS

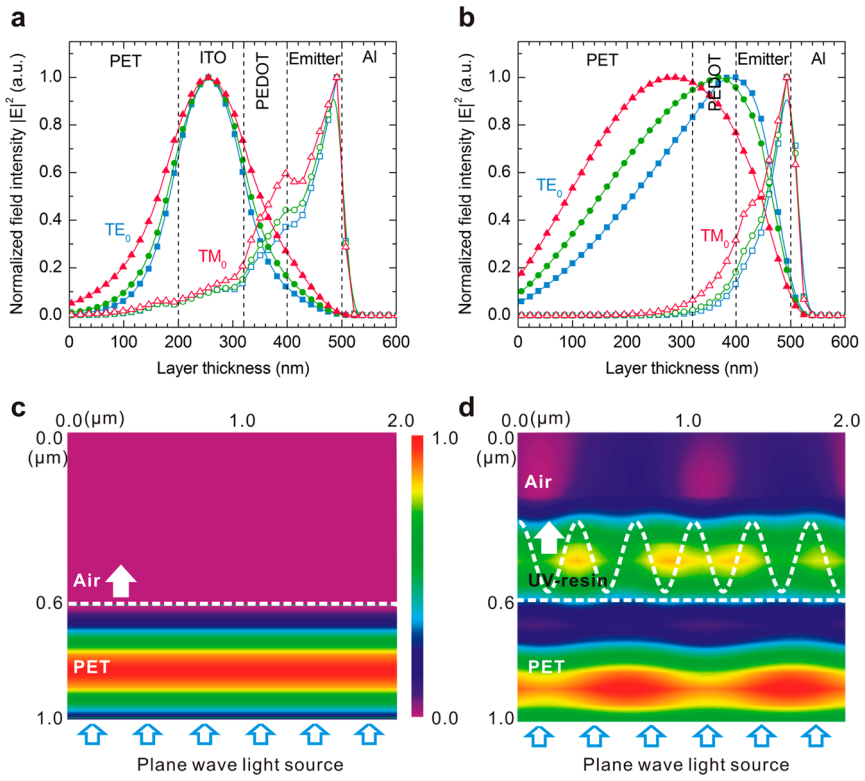

Figure 5. Simulated distributions of electric field intensity by the FDTD method. (a, b) Distributions of electric field intensity for TE_0 and TM_0 modes at λ = 470, 520, and 610 nm in FOLEDs on (a) ITO/PET and (b) PET-AN/OC, respectively. (c, d) Field intensity distributions of plane wave light at λ = 520 nm passing through the flat PET (c) without and (d) with a moth-eye outcoupling layer. The arrows depict the energy flow direction. The white dashed lines represent the interface of different layers.

layer ($n_{PEDOT} \approx 1.5$) as compared to the high-refractive-index ITO layer ($n_{ITO} \approx 1.8-2.1$).[47] As a result, a considerable fraction of the emitted photons originally confined in the ITO/organic waveguide mode can be efficiently outcoupled into the PET substrate, which is beneficial for the overall outcoupling enhancement of FOLEDs due to the efficient extraction of light trapped in the substrate modes using a moth-eye OC layer on the outer surface of the flexible plastic substrate. This finding is consistent with the experimental results of the enhanced light outcoupling efficiency and EQE values for FOLEDs using PET-AN/OC in comparison with standard devices on ITO-coated substrates (Figures 2 and 3).

Besides the elimination of the ITO/organic waveguide modes due to the replacement of the ITO layer, the effect of the moth-eye OC layer on the optical extraction in FOLEDs using PET-AN/OC is analyzed by modeling the field distribution at the substrate/air interfaces. As depicted in Figure 5c and d, the optical modeling qualitatively shows the relatively stronger electric field intensity on the nanostructured surface rather than that of the bare PET substrate, revealing the more efficient light extraction of the PET-AN/OC substrate. According to the previous reports,[48−50] the subwavelength OC layer with moth-eye nanostructures on glass and PET substrates can dramatically enhance the optical coupling due to the gradient refractive index distribution at the substrate/air interface. Therefore, the overall light outcoupling and external quantum efficiencies of FOLEDs using a PET-AN/OC substrate can be enhanced over the device with a conventional ITO electrode.

CONCLUSIONS

In conclusion, we demonstrate a simple and novel method to synergistically optimize both light outcoupling and hole injection efficiencies in FOLEDs by developing an ameliorated plastic substrate with low refractive index that consists of a bioinspired optical coupling layer and a built-in silver network transparent electrode. This new flexible plastic substrate enables the good transmittance to full-color emission (>94% over the whole visible wavelength range), a highly conductive channel for charge transport (sheet resistance <5 Ω sq^{-1}), and high tolerance to mechanical bending. The angularly and spectrally independent enhancement of light outcoupling is realized in FOLEDs. As a result, FOLEDs using PET-AN/OC yield PE values of 47, 93, 56, and 52 lm W^{-1} for red, green, blue, and white emissions, respectively, which are competitive with a conventional OLED constructed on standard ITO-coated glass substrates. Furthermore, superior angular color stability of white FOLEDs is observed,

where the diverse emission spectra are strongly suppressed regardless of the viewing angle. These achievements reveal a great potential of using PET-AN/OCs in large-area next-generation ITO-free flexible technologies for full-color displays and solid-state lighting.

METHODS

Device Fabrication. The flexible plastic substrates were ultrasonically cleaned with detergent, acetone, ethanol, and DI water for 20 min and finally dried in an oven. The built-in Ag network TCE was fabricated on a PET substrate by ingeniously combining Ag paste scratch technology, nanoimprinting lithography, and precise pattern photolithography (Supporting Figure S1). The resulting PET-AN/OC substrate was cleaned by ethanol and dried in an oven in succession. A 80 nm thick PEDOT:PSS (with 5 vol % dimethy1-sulfoxide to increase the conductivity and mixed with 0.5 vol % Zonyl FS-300 fluorosurfactant from Fluka to promote wetting on the UV-curable resin-coated PET substrate) was spin-coated onto the ultraviolet-ozone-treated ITO/PET and PET-AN/OC substrates under ambient conditions, which was followed by heat treatment at 80 °C for 20 min prior to subsequent layer deposition. To prepare the moth-eye antireflection layer on the outer surface of the PET substrate, a UV-assisted nanoimprinting method was introduced with a flexible polydimethylsiloxane mold on the basis of soft nanoimprint lithography under atmospheric conditions, which resulted in the formation of the high-profile three-dimensional subwavelength patterns. The substrates with a PEDOT:PSS layer were transferred into a high-vacuum evaporation chamber (base pressure $<5 \times 10^{-7}$ Torr) with computer-controlled shadow masks for film deposition. For the OLED fabrication, organic layers and a LiF/Al bilayer cathode were thermally deposited with a base pressure of 2×10^{-6} Torr, and the deposition rate and film thickness were monitored by a quartz crystal oscillator. The emission areas of flexible OLEDs were 144 mm^2 on PET-AN/OC, PET-AN, and ITO/PET and 10 mm^2 on ITO/glass substrates. To ensure consistent results, the devices on various substrates were fabricated in the same vacuum chamber at the same time. The main materials used have acronyms as follows. FIrpic: bis(3,5-difluoro-2-(2-pyridyl)phenyl-(2-carboxypyridyl) iridium(III) as blue emitter. Ir(ppy)$_2$(acac): bis(2-phenylpyridine) (acetylacetonate) iridium(III) as green emitter. Ir(MDQ)$_2$(acac): bis(2-methyldibenzo[*f*,*h*]-quinoxaline) (acetylacetonate) iridium(III) as red emitter. NPB: *N*,*N*′-bis(naphthalen-1-yl)-*N*,*N*′-bis(phenyl)-benzidine as the hole transport layer. TCTA: 4,4′,4″-tris(*N*-carbazolyl)-triphenylamine as the electron/exciton blocking layer. TmPyPB: 1,3,5-tris(*m*-pyrid-3-ylphenyl)benzene as the electron transport layer and the hole/exciton blocking layer. Detailed device structures are as follow.

Red FOLED: anode/PEDOT:PSS (80 nm)/NPB (40 nm)/TCTA (15 nm) /Ir(MDQ)$_2$(acac) (0.1 nm)/TmPyPB (30 nm)/LiF (1 nm)/Al (100 nm).

Green FOLED: anode/PEDOT:PSS (80 nm)/NPB (40 nm)/TCTA (15 nm)/Ir(ppy)$_2$(acac) (0.1 nm)/TmPyPB (30 nm)/LiF (1 nm)/Al (100 nm).

Blue FOLED: anode/PEDOT:PSS (80 nm)/NPB (40 nm)/TCTA (15 nm)/FIrpic (0.1 nm)/TmPyPB (30 nm)/LiF (1 nm)/Al (100 nm).

White FOLED: anode/PEDOT:PSS (80 nm)/NPB (40 nm)/TCTA (13 nm)/Ir(MDQ)$_2$(acac) (0.1 nm)/TCTA (1 nm)/Ir(ppy)$_2$(acac) (0.05 nm)/TCTA (1 nm)/FIrpic (0.1 nm)/TmPyPB (40 nm)/LiF (1 nm)/Al (100 nm).

Device Characterization. The current density−voltage−luminance characteristics and electroluminescence spectra of the corresponding devices were measured simultaneously in air ambience using a computer-controlled programmable Keithley model 2400 power source and a PhotoResearch PR 655 spectrometer. The angle-dependent emission spectra and light intensity were characterized by placing the devices on a rotating stage with one of the grooves parallel to the rotation axis. The refractive index (*n*) and extinction coefficient (*k*) of all the films were measured using an Alpha-SE spectroscopic ellipsometer (J.A. Woollam Co., Inc.). The film thickness was measured by the Alpha-SE spectroscopic ellipsometer. Transmission spectra were recorded by a UV/vis/near-IR spectrophotometer (PerkinElmer Lambda 750) with an integrating sphere. Surface morphology was characterized with AFM (Veeco MultiMode V). The sheet resistances of different TCEs were measured using a digital multimeter (Keithley 2100) with a four-point probe configuration to eliminate contact resistance.

Theoretical Modeling. For devices with subwavelength patterning, geometric optics based on the ray tracing method cannot be used for simulating the photon flux distribution in nanoscale optical fields. To simulate the field radiation pattern of TE and TM polarized light in FOLEDs on various flexible substrates, the FDTD method was adopted using a commercial FDTD solver (Lumerical FDTD Solutions 8.7.3), in which hexagonal closely packed nanostructures with a continuously tapered profile were used for simplicity instead of a randomly distributed geometry. In the modeling, electrical dipole oscillators were put inside the FOLEDs. The complex optical dielectric function of the nanostructured Al cathode was fitted using the Lorentz−Drude model, taking into account the interband transitions. The frequency-dependent *n* and *k* of PEDOT:PSS, ITO, and PET experimentally measured by ellipsometer were used as experimental input parameters for calculations.

Conflict of Interest: The authors declare no competing financial interest.

Acknowledgment. The authors acknowledge financial support from the National Basic Research Program of China (Grant No. 2014CB932600), the National Natural Science Foundation of China (Grant Nos. 91433116, 91323303, 11474214, 612111116), Jiangsu Science and Technology Department (Grant No. BK20140053), Bureau of Science and Technology of Suzhou Municipality (Grant No. ZXG201422), and the project of the Priority Academic Program Development (PAPD) of Jiangsu Higher Education Institutions.

Supporting Information Available: Basic information about the fabrication process for ameliorated plastic with an embedded Ag network, a comparison of optical and mechanical properties of various flexible substrates, and the current efficiencies of flexible devices with red, green, and blue are also presented. The Supporting Information is available free of charge on the ACS Publications website at DOI: 10.1021/acsnano.5b02826.

REFERENCES AND NOTES

1. Zeng, X. Y.; Zhang, Q. K.; Yu, R. M.; Lu, C. Z. A New Transparent Conductor: Silver Nanowire Film Buried at the Surface of a Transparent Polymer. *Adv. Mater.* **2010**, *22*, 4484–4488.
2. Wang, Z. B.; Helander, M. G.; Qiu, J.; Puzzo, D. P.; Greiner, M. T.; Hudson, Z. M.; Wang, S.; Liu, Z. W.; Lu, Z. H. Unlocking the Full Potential of Organic Light-Emitting Diodes on Flexible Plastic. *Nat. Photonics* **2011**, *5*, 753–757.
3. Sandström, A.; Dam, H. F.; Krebs, F. C.; Edman, L. Ambient Fabrication of Flexible and Large-Area Organic Light-Emitting Devices Using Slot-Die Coating. *Nat. Commun.* **2012**, *3*, 1002.
4. Sugimoto, A.; Ochi, H.; Fujimura, S.; Yoshida, A.; Miyadera, T.; Tsuchida, M. Flexible OLED Displays Using Plastic Substrates. *IEEE J. Sel. Top. Quantum Electron.* **2004**, *10*, 107–114.
5. Cai, M.; Ye, Z.; Xiao, T.; Liu, R.; Chen, Y.; Mayer, R. W.; Biswas, R.; Ho, K. M.; Shinar, R.; Shinar, J. Extremely Efficient Indium-Tin-Oxide-Free Green Phosphorescent Organic Light-Emitting Diodes. *Adv. Mater.* **2012**, *24*, 4337–4342.
6. Peng, C.; Jia, Z.; Neilson, H.; Li, T.; Lou, J. *In Situ* Electro-Mechanical Experiments and Mechanics Modeling of

Fracture in Indium Tin Oxide-Based Multilayer Electrodes. *Adv. Eng. Mater.* **2013**, *15*, 250–256.
7. Kim, Y. H.; Sachse, C.; Machala, M. L.; May, C.; Müller-Meskamp, L.; Leo, K. Highly Conductive PEDOT: PSS Electrode with Optimized Solvent and Thermal Post-Treatment for ITO-Free Organic Solar Cells. *Adv. Funct. Mater.* **2011**, *21*, 1076–1081.
8. Han, T. H.; Lee, Y.; Choi, M. R.; Woo, S. H.; Bae, S. H.; Hong, B. H.; Ahn, J. H.; Lee, T. W. Extremely Efficient Flexible Organic Light-Emitting Diodes with Modified Graphene Anode. *Nat. Photonics* **2012**, *6*, 105–110.
9. Kim, K. S.; Zhao, Y.; Jang, H.; Lee, S. Y.; Kim, J. M.; Kim, K. S.; Ahn, J. H.; Kim, P.; Choi, J. Y.; Hong, B. H. Large-Scale Pattern Growth of Graphene Films for Stretchable Transparent Electrodes. *Nature* **2009**, *457*, 706–710.
10. Hecht, D. S.; Hu, L. B.; Irvin, G. Emerging Transparent Electrodes Based on Thin Films of Carbon Nanotubes, Graphene, and Metallic Nanostructures. *Adv. Mater.* **2011**, *23*, 1482–1513.
11. Freitag, P.; Zakhidov, A. A.; Luessem, B.; Zakhidov, A. A.; Leo, K. Lambertian White Top-Emitting Organic Light Emitting Device with Carbon Nanotube Cathode. *J. Appl. Phys.* **2012**, *112*, 114505.
12. Guo, H. Z.; Lin, N.; Chen, Y. Z.; Wang, Z. W.; Xie, Q. S.; Zheng, T. C.; Gao, N.; Li, S. P.; Kang, J. Y.; Cai, D. J.; *et al*. Copper Nanowires as Fully Transparent Conductive Electrodes. *Sci. Rep.* **2013**, *3*, 1038.
13. Rathmell, A. R.; Bergin, S. M.; Hua, Y. L.; Li, Z. Y.; Wiley, B. J. The Growth Mechanism of Copper Nanowires and Their Properties in Flexible, Transparent Conducting Films. *Adv. Mater.* **2010**, *22*, 3558–3563.
14. Gaynor, W.; Lee, J. Y.; Peumans, P. Fully Solution-Processed Inverted Polymer Solar Cells with Laminated Nanowire Electrodes. *ACS Nano* **2010**, *4*, 30–34.
15. Yu, Z. B.; Zhang, Q. W.; Li, L.; Chen, Q.; Niu, X. F.; Liu, J.; Pei, Q. B. Highly Flexible Silver Nanowire Electrodes for Shape-Memory Polymer Light-Emitting Diodes. *Adv. Mater.* **2011**, *23*, 664–668.
16. Kim, S. J.; Yu, H. K.; Hong, K.; Kim, K.; Son, J. H.; Lee, I.; Kim, K. B.; Kim, T. Y.; Lee, J. L. MgO Nano-Facet Embedded Silver-Based Dielectric/Metal/Dielectric Transparent Electrode. *Opt. Express* **2012**, *20*, 845–853.
17. Cho, H.; Yun, C. H.; Yoo, S. Multilayer Transparent Electrode For Organic Light-Emitting Diodes: Tuning Its Optical Characteristics. *Opt. Express* **2010**, *18*, 3404–3414.
18. Cho, H.; Yun, C. H.; Park, J. W.; Yoo, S. Highly Flexible Organic Light-Emitting Diodes Based on ZnS/Ag/WO_3 Multilayer Transparent Electrodes. *Org. Electron.* **2009**, *10*, 1163–1169.
19. Carlé, J. E.; Andersen, T. R.; Helgesen, M.; Bundgaard, E.; Jørgensen, M.; Krebs, F. C. A Laboratory Scale Approach to Polymer Solar Cells Using One Coating/Printing Machine, Flexible Substrates, No ITO, No Vacuum and No Spincoating. *Sol. Energy Mater. Sol. Cells* **2013**, *108*, 126–128.
20. Huang, Y. C.; Hsu, F. H.; Cha, H. C.; Chuang, C. M.; Tsao, C. S.; Chen, C. Y. High-Performance ITO-Free Spray-Processed Polymer Solar Cells with Incorporating Inkjet Printed Grid. *Org. Electron.* **2013**, *14*, 2809–2817.
21. Kang, M. G.; Guo, L. J. Nanoimprinted Semitransparent Metal Electrodes and Their Application in Organic Light-Emitting Diodes. *Adv. Mater.* **2007**, *19*, 1391–1396.
22. Galagan, Y.; Zimmermann, B.; Coenen, E. W. C.; Jørgensen, M.; Tanenbaum, D. M.; Krebs, F. C.; Gorter, H.; Sabik, S.; Slooff, L. H.; Veenstra, S. C. Current Collecting Grids for ITO-Free Solar Cells. *Adv. Energy Mater.* **2012**, *2*, 103–110.
23. Van Osch, T. H.; Perelaer, J.; de Laat, A. W.; Schubert, U. S. Inkjet Printing of Narrow Conductive Tracks on Untreated Polymeric Substrates. *Adv. Mater.* **2008**, *20*, 343–345.
24. Ahn, B. Y.; Duoss, E. B.; Motala, M. J.; Guo, X. Y.; Park, S. I.; Xiong, Y. J.; Yoon, J.; Nuzzo, R. G.; Rogers, J. A.; Lewis, J. A. Omnidirectional Printing of Flexible, Stretchable, and Spanning Silver Microelectrodes. *Science* **2009**, *323*, 1590–1593.
25. Aernouts, T.; Vanlaeke, P.; Geens, W.; Poortmans, J.; Hermans, P.; Borghs, S.; Mertens, R.; Andriessen, R.; Leenders, L. Printable Anodes for Flexible Organic Solar Cell Modules. *Thin Solid Films* **2004**, *451*, 22–25.
26. Chutinan, A.; Ishihara, K.; Asano, T.; Fujita, M.; Noda, S. Theoretical Analysis on Light-Extraction Efficiency of Organic Light-Emitting Diodes Using FDTD and Mode-Expansion Methods. *Org. Electron.* **2005**, *6*, 3–9.
27. Sun, Y.; Forrest, S. R. Enhanced Light Out-Coupling of Organic Light-Emitting Devices Using Embedded Low-Index Grids. *Nat. Photonics* **2008**, *2*, 483–487.
28. Reineke, S.; Lindner, F.; Schwartz, G.; Seidler, N.; Walzer, K.; Lussem, B.; Leo, K. White Organic Light-Emitting Diodes with Fluorescent Tube Efficiency. *Nature* **2009**, *459*, 234–238.
29. Koo, W. H.; Jeong, S. M.; Araoka, F.; Ishikawa, K.; Nishimura, S.; Toyooka, T.; Takezoe, H. Light Extraction from Organic Light-Emitting Diodes Enhanced by Spontaneously Formed Buckles. *Nat. Photonics* **2010**, *4*, 222–226.
30. Lee, C.; Kim, J. J. Enhanced Light Out-Coupling of OLEDs with Low Haze by Inserting Randomly Dispersed Nanopillar Arrays Formed by Lateral Phase Separation of Polymer Blends. *Small* **2013**, *9*, 3858–3863.
31. Zhou, L.; Ou, Q. D.; Chen, J. D.; Shen, S.; Tang, J. X.; Li, Y. Q.; Lee, S. T. Light Manipulation for Organic Optoelectronics with Bio-Inspired Moth's Eye Nanostructures. *Sci. Rep.* **2014**, *4*, 4040.
32. Ding, W.; Wang, Y.; Chen, H.; Chou, S. Y. Plasmonic Nanocavity Organic Light-Emitting Diode with Significantly Enhanced Light Extraction, Contrast, Viewing Angle, Brightness, and Low-Glare. *Adv. Funct. Mater.* **2014**, *24*, 6329–6340.
33. Ou, Q. D.; Zhou, L.; Li, Y. Q.; Shen, S.; Chen, J. D.; Li, C.; Wang, Q. K.; Lee, S. T.; Tang, J. X. Extremely Effi cient White Organic Light-Emitting Diodes for General Lighting. *Adv. Funct. Mater.* **2014**, *24*, 7249–7256.
34. Kim, E.; Cho, H.; Kim, K.; Koh, T. W.; Chung, J.; Lee, J.; Park, Y. K.; Yoo, S. A Facile Route to Effi cient, Low-Cost Flexible Organic Light-Emitting Diodes: Utilizing the High Refractive Index and Built-In Scattering Properties of Industrial-Grade PEN Substrates. *Adv. Mater.* **2015**, *27*, 1624–1631.
35. Mladenovski, S.; Neyts, K.; Pavicic, D.; Werner, A.; Rothe, C. Exceptionally Efficient Organic Light Emitting Devices Using High Refractive Index Substrates. *Opt. Express* **2009**, *17*, 7562–7570.
36. Chen, J. D.; Zhou, L.; Ou, Q. D.; Li, Y. Q.; Shen, S.; Lee, S. T.; Tang, J. X. Enhanced Light Harvesting in Organic Solar Cells Featuring a Biomimetic Active Layer and a Self-Cleaning Antireflective Coating. *Adv. Energy Mater.* **2014**, *4*, 1301777.
37. Martins, E. R.; Li, J.; Liu, Y. K.; Depauw, V.; Chen, Z.; Zhou, J.; Krauss, T. F. Deterministic Quasi-random Nanostructures for Photon Control. *Nat. Commun.* **2013**, *4*, 2665.
38. Villani, F.; Vacca, P.; Nenna, G.; Valentino, O.; Burrasca, G.; Fasolino, T.; Minarini, C.; della Sala, D. Inkjet Printed Polymer Layer on Flexible Substrate for OLED Applications. *J. Phys. Chem. C* **2009**, *113*, 13398–13402.
39. Leem, D. S.; Edwards, A.; Faist, M.; Nelson, J.; Bradley, D. D. C.; de Mello, J. C. Efficient Organic Solar Cells with Solution-Processed Silver Nanowire Electrodes. *Adv. Mater.* **2011**, *23*, 4371–4375.
40. Geng, H. Z.; Kim, K. K.; So, K. P.; Lee, Y. S.; Chang, Y.; Lee, Y. H. Effect of Acid Treatment on Carbon Nanotube-Based Flexible Transparent Conducting Films. *J. Am. Chem. Soc.* **2007**, *129*, 7758–7759.
41. Lee, J. Y.; Connor, S. T.; Cui, Y.; Peumans, P. Solution-Processed Metal Nanowire Mesh Transparent Electrodes. *Nano Lett.* **2008**, *8*, 689–692.
42. Bae, S.; Kim, H.; Lee, Y. B.; Xu, X. F.; Park, J. S.; Zheng, Y.; Balakrishnan, J.; Lei, T.; Kim, H. R.; Song, Y. I. Roll-to-Roll Production of 30-Inch Graphene Films for Transparent Electrodes. *Nat. Nanotechnol.* **2010**, *5*, 574–578.
43. Zhao, Y.; Chen, J.; Ma, D. G. Ultrathin Nondoped Emissive Layers for Efficient and Simple Monochrome and White Organic Light-Emitting Diodes. *ACS Appl. Mater. Interfaces* **2013**, *5*, 965–971.
44. Wang, Q.; Oswald, I. W. H.; Yang, X. L.; Zhou, G. J.; Jia, H. P.; Qiao, Q. Q.; Chen, Y. H.; Hoshikawa-Halbert, J.; Gnade, B. E.

A Non-Doped Phosphorescent Organic Light-Emitting Device with Above 31% External Quantum Efficiency. *Adv. Mater.* **2014**, *26*, 8107–8113.
45. Gaynor, W.; Hofmann, S.; Christoforo, M. G.; Sachse, C.; Mehra, S.; Salleo, A.; McGehee, M. D.; Gather, M. C.; Lüssem, B.; Müller-Meskamp, L. Color in the Corners: ITO-Free White OLEDs with Angular Color Stability. *Adv. Mater.* **2013**, *25*, 4006–4013.
46. Zhou, L.; Jiang, X. C.; Li, Y. Q.; Shi, A. L.; Chen, J. D.; Ou, Q. D.; Liu, H. T.; Tang, J. X. Light Extraction of Trapped Optical Modes in Polymer Light-Emitting Diodes with Nanoimprinted Double-Pattern Gratings. *ACS Appl. Mater. Interfaces* **2014**, *6*, 18139–18146.
47. Huang, Y. H.; Lu, C. Y.; Tsai, S. T.; Tsai, Y. T.; Chen, C. Y.; Tsai, W. L.; Lin, C. Y.; Chang, H. W.; Lee, W. K.; Jiao, M.; *et al*. Enhancing Light Out-Coupling of Organic Light-Emitting Devices Using Indium Tin Oxide-Free Low-Index Transparent Electrodes. *Appl. Phys. Lett.* **2014**, *104*, 183302.
48. Parker, A. R.; Townley, H. E. Biomimetics of Photonic Nanostructures. *Nat. Nanotechnol.* **2007**, *2*, 347–353.
49. Yu, P. C.; Chang, C. H.; Chiu, C. H.; Yang, C. S.; Yu, J. C.; Kuo, H. C.; Hsu, S. H.; Chang, Y. C. Efficiency enhancement of GaAs photovoltaics employing antireflective indium tin oxide nanocolumns. *Adv. Mater.* **2009**, *21*, 1618–1621.
50. Song, Y. M.; Park, G. C.; Jang, S. J.; Ha, J. H.; Yu, J. S.; Lee, Y. T. Multifunctional Light Escaping Architecture Inspired by Compound Eye Surface Structures: From Understanding to Experimental Demonstration. *Opt. Express* **2011**, *19*, A157–A165.